

# Quantifying nonadiabaticity in major families of superconductors

Evgeny F. Talantsev<sup>1,2\*</sup>

<sup>1</sup>M.N. Miheev Institute of Metal Physics, Ural Branch, Russian Academy of Sciences,  
18, S. Kovalevskoy St., Ekaterinburg, 620108, Russia

<sup>2</sup>NANOTECH Centre, Ural Federal University, 19 Mira St., Ekaterinburg, 620002, Russia

## Abstract

The classical Bardeen-Cooper-Schrieffer and Eliashberg theories of the electron–phonon-mediated superconductivity are based on the Migdal theorem, which is an assumption that the energy of charge carriers,  $k_B T_F$ , significantly exceeds the phononic energy,  $\hbar\omega_D$ , of the crystalline lattice. This assumption, which is also known as adiabatic approximation, implies that the superconductor exhibits fast charge carriers and slow phonons. This picture is valid for pure metals and metallic alloys because these superconductors exhibit  $\frac{\hbar\omega_D}{k_B T_F} < 0.01$ . However, *n*-type doped semiconducting SrTiO<sub>3</sub> was the first superconductor which beyond this adiabatic approximation, because this material exhibit  $\frac{\hbar\omega_D}{k_B T_F} \cong 50$ . There is growing number of newly discovered superconductors which also beyond the adiabatic approximation. Here, leaving apart pure theoretical aspects of nonadiabatic superconductors, we classified major classes of superconductors (including, elements, A-15 and Heusler alloys, Laves phases, intermetallics, noncentrosymmetric compounds, cuprates, pnictides, highly-compressed hydrides and oxygen, and magic-angle twisted bilayer graphene) by the strength of nonadiabaticity (for which the ratio of the Debye temperature to the Fermi temperature,  $\frac{T_\theta}{T_F}$ , is used as a criterion for the nonadiabaticity) versus the superconducting transition temperature,  $T_c$ . The discussion of this classification scheme and its relation to other known classification counterparts is given.

## Quantifying nonadiabaticity in major families of superconductors

### 1. Introduction

The majority of experimental works in superconductivity utilizes classical the Bardeen-Cooper-Schrieffer (BCS) [1] and the Migdal-Eliashberg (ME) [2,3] theories as primary tool to analyse measured data. However, as this was pointed out by Pietronero and coworkers [4], that these theories are valid for superconductors which satisfy the condition designated as Born-Oppenheimer-Migdal approximation [4]:

$$\frac{\hbar\omega_D}{k_B T_F} = \frac{T_\theta}{T_F} = \left. \frac{88 K}{1.1 \times 10^5 K} \right|_{Pb} = 8 \times 10^{-4} \ll 1, \quad (1)$$

where  $\hbar$  is reduced Planck constant,  $\omega_D$  is the Debye frequency,  $k_B$  the Boltzmann constant,  $T_\theta$  is the Debye temperature,  $T_F$  is the Fermi temperature, and data for lead reported by Poole [5]. Born-Oppenheimer-Migdal approximation allows to separate electronic and ionic motions in metals, because Eq. 1 implies that the conductor exhibits fast charge carriers (for which characteristic energy scale is related to the Fermi temperature,  $T_F$ ) and relatively slow phonons (for which characteristic energy scale is related to the Debye temperature,  $T_\theta$ ).

However, Eq. 1 satisfies for many, but not for all superconductors, and the first discovered superconductor for which Eq. 1 was found to be violated is *n*-type doped semiconducting SrTiO<sub>3</sub> [6]:

$$\frac{\hbar\omega_D}{k_B T_F} = \frac{T_\theta}{T_F} = \left. \frac{627 K}{13 K} \right|_{SrTiO_3} = 48 \gg 1, \quad (2)$$

where data for SrTiO<sub>3</sub> is taken from [7,8]. Theoretical description of the superconductivity in materials, in which the charge carriers and the lattice vibrations exhibit similar to Eq. 2 characteristic energy scales is complicated and general designation of this superconductors is nonadiabatic superconductors [9-16]. The theory [9-16] provides general equation for the superconducting transition temperature,  $T_c$ , in nonadiabatic superconductors [9]:  $T_c = 1.134 \times$

$\frac{\varepsilon_F}{k_B} \times e^{-\frac{1}{\lambda_{nad}}}$ , where  $\varepsilon_F$  is the Fermi energy, and  $\lambda_{nad}$  is the coupling strength constant in

nonadiabatic superconductors, which serves similar role to the electron-phonon coupling strength,  $\lambda_{e-ph}$ , in the BCS [1] and ME [2,3] theories. And one of the primary fundamental theoretical problem is to calculate this constant with acceptable accuracy to describe the experiment [4-16].

For experimentalists, it is important to have simple practical routine to establish the strength of nonantiadiabatic effects in newly discovered superconductor. The most obvious parameter, which can be served as experimentally measured value to quantify the strength of nonantiadiabaticity is the  $\frac{T_\theta}{T_F}$  ratio. For practical use of this criterion, there is a need for the taxonomy of possible  $\frac{T_\theta}{T_F}$  values.

In this paper we analysed experimental data for major families of superconductors and based on our analysis we proposed the following classification scheme:

$$\begin{cases} \frac{T_\theta}{T_F} < 0.025 \rightarrow \text{adiabatic superconductor}; \\ 0.025 \lesssim \frac{T_\theta}{T_F} \lesssim 0.4 \rightarrow \text{moderate nonadiabaticity}; \\ 0.4 < \frac{T_\theta}{T_F} \rightarrow \text{nonadiabatic superconductor}; \end{cases} \quad (3)$$

One of our findings is that for weakly nonadiabatic superconductors (i.e. for materials exhibited  $0.025 \leq \frac{T_\theta}{T_F} \lesssim 0.4$ ) the predicting power of the BCS-ME theories (for instance, the prediction of the superconducting transition temperature) is reasonably accurate. However, all these superconductors are located outside of the BCS corner in the Uemura plot.

We also showed how the proposed classification scheme is linked to some other known empirical scaling laws and taxonomies in superconductivity [13,17-21], while the search for the link of the proposed taxonomy with recently reported big data [22,23] is under a progress.

## 2. Utilized models

Proposed taxonomy is based on the knowledge of three fundamental temperatures of the superconductor, which are  $T_c$ ,  $T_\theta$ , and  $T_F$ . The superconducting transition temperature,  $T_c$ , is directly measured in either temperature resistance, either in magnetization, experiments, and it is important to mention primary experimental techniques and theoretical models utilized to deduce the Debye temperature,  $T_\theta$ , and the Fermi temperature,  $T_F$ , in superconductors.

There are two primary techniques to determine the Debye temperature,  $T_\theta$ . One technique is to analyse measured the temperature dependent normal-state specific heat,  $C_p(T)$ , from which the electronic specific heat coefficient,  $\gamma_n$ , and the Debye temperature,  $T_\theta$ , are deduced (see, for instance [24-26]):

$$\frac{C_p(T)}{T} = \gamma_n + \beta T^2 + \alpha T^4 \quad (4)$$

where  $\beta$  is the Debye law lattice heat-capacity contribution, and  $\alpha$  is from higher-order lattice contributions. The Debye temperature can be calculated using:

$$T_\theta = \left( \frac{12\pi^4 R p}{5\beta} \right)^{\frac{1}{3}} \quad (5)$$

where  $R$  is the molar gas constant, and  $p$  is the number of atoms per formula unit.

Another technique is to fit normal-state temperature dependent resistance,  $R(T)$ , to the Bloch-Grüneisen (BG) equation [24-28]:

$$R(T) = \frac{1}{\frac{1}{R_{sat}} + \frac{1}{R_0 + A \times \left(\frac{T}{T_\theta}\right)^5 \times \int_0^{\frac{T_\theta}{T}} \frac{x^5}{(e^x - 1)(1 - e^{-x})} dx}} \quad (6)$$

where,  $R_{sat}$  is the saturated resistance at high temperatures which is temperature independent,  $R_0$  is the residual resistance at  $T \rightarrow 0 K$ , and  $A$  is free fitting parameter. Many research groups utilized both techniques (i.e. Eqs. 4-6) to deduce  $T_\theta$  [24-27,29].

From measured  $T_c$  and deduced  $T_\theta$ , one can derived the electron-phonon coupling constant,  $\lambda_{e-ph}$ , as a root of either original McMillan equation [30], either its recently revisited form [27]:

$$T_c = \left(\frac{1}{1.45}\right) \times T_\theta \times e^{-\left(\frac{1.04(1+\lambda_{e-ph})}{\lambda_{e-ph}-\mu^*(1+0.62\lambda_{e-ph})}\right)} \times f_1 \times f_2^* \quad (7)$$

$$f_1 = \left(1 + \left(\frac{\lambda_{e-ph}}{2.46(1+3.8\mu^*)}\right)^{3/2}\right)^{1/3} \quad (8)$$

$$f_2^* = 1 + (0.0241 - 0.0735 \times \mu^*) \times \lambda_{e-ph}^2 \quad (9)$$

where  $\mu^*$  is the Coulomb pseudopotential,  $0.10 \lesssim \mu^* \lesssim 0.15$  [27,30].

There are several experimental techniques to derive the Fermi temperature,  $T_F$ , from experimental data. One of these techniques is to measure temperature dependent Seebeck coefficient,  $S(T)$ , and fit measured dataset to the equation [8]:

$$\left|\frac{S(T)}{T}\right| = \frac{\pi^2}{3} \frac{k_B}{e} \frac{1}{T_F} \quad (10)$$

Another approach is to measure the magnetic quantum oscillations [31] from which the magnitude of charge carrier mass,  $m^* = m_e(1 + \lambda_{e-ph})$  (where  $m_e$  is bare mass od electron), together with the size of the Fermi wave vector,  $k_F$ , can be obtained and plugged into [31]:

$$T_F = \frac{\hbar^2}{2k_B} \frac{k_F^2}{m^*} \quad (11)$$

Alternative approach is based on the extracting of the charge carriers mass,  $m^*$ , and density,  $n$ , as two of four parameters from the simultaneous analysis of  $C_p(T)$ ,  $R(T)$ , the muon spin relaxation ( $\mu$ SR), the lower critical field data,  $B_{c1}(T)$ , and the upper critical field data,  $B_{c2}(T)$  [32], and plugging these parameters into equation for isotropic spherical Fermi surface [32]:

$$T_F = \frac{\hbar^2}{2k_B} \frac{1}{m^*} (3\pi^2 n_s)^{\frac{2}{3}} \quad (12)$$

where  $n_s$  is bulk charge carriers density at  $T \rightarrow 0 K$ . For 3D superconductors,  $n_s$  is given by the equation [33]:

$$n_s(0) = \frac{m^*}{\mu_0 e^2} \frac{1}{\lambda^2(0)}, \quad (13)$$

where  $\mu_0$  is the permeability of free space,  $l$  is the charge carrier mean free path,  $\lambda(0)$  is the ground state London penetration depth, and  $\xi(0)$  is the ground state coherence length.

It should be noted, that  $\lambda(0)$  can be also deduced from the ground state lower critical field [28,34]:

$$B_{c1}(0) = \frac{\phi_0}{4\pi} \frac{\ln(1+\sqrt{2}\kappa(0))}{\lambda^2(0)}, \quad (14)$$

where  $\kappa(0) = \frac{\lambda(0)}{\xi(0)}$  is the ground state Ginzburg-Landau parameter.

For two dimensional (2D) superconductors,  $T_F$  can be determined from  $\mu$ SR measurements and crystallographic data [18]:

$$T_F = \frac{\pi\hbar^2}{k_B m^*} \frac{1}{n_s} c_{int}, \quad (15)$$

where  $c_{int}$  is the average distance between superconducting planes.

If measuring techniques are limited to the magnetoresistance measurements,  $R(T, B)$  (which was the case in the field of highly-compressed near-room temperature superconductors (NRTS) [35-50], until recent experimental progress by Minkov *et al* [51,52]),  $T_F$  can be estimated by the equation [53]:

$$T_F = \frac{\pi^2 m^*}{2k_B \hbar^2} \times \xi^2(0) \times \Delta^2(0), \quad (16)$$

where  $\Delta(0)$  is the ground state amplitude of the superconducting energy gap, which is varying in reasonably narrow range  $3.2 \leq \frac{2\Delta(0)}{k_B T_c} \leq 5.0$ , that the ballpark value for  $T_F$  can be estimated.

### 3. Results

In Table 1 we presented data for major groups of superconductors, where data sources for  $T_c$ ,  $T_\theta$ ,  $T_F$ , and other parameters (for instance,  $\lambda_{e-ph}$ ) are given.

In Figure 1 we showed  $T_c$  vs  $T_F$  dataset in log-log plot, which is traditional data representation in well-known Uemura plot [18].

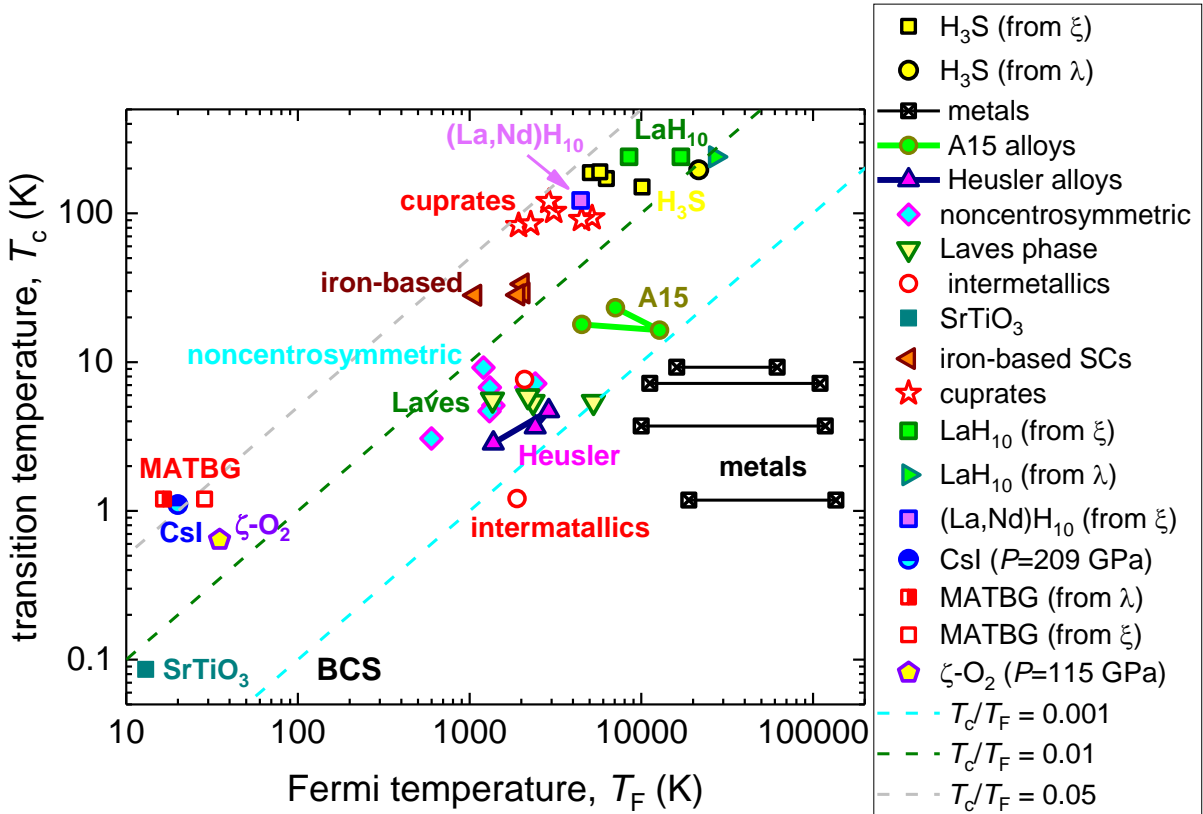


**Figure 1.** Uemura plot ( $T_c$  vs  $T_F$ ) for primary superconducting families. References on original data ( $T_c$  and  $T_F$ ) can be found in Table 1.

In Figure 2 we represented same superconducting materials, but here we displayed  $\lambda_{e-ph}$  vs  $\frac{T_\theta}{T_F}$  dataset in semi-log plot. For our best knowledge,  $\lambda_{e-ph}$  vs  $\frac{T_\theta}{T_F}$  plot was first plotted by Pietronero *et al* [13] in linear-linear scales. However, because  $\frac{T_\theta}{T_F}$  ratio for main families of superconductors is varied within four orders of magnitude (Table 1), and  $0.4 \leq \lambda_{e-ph} \leq 3.0$  it is more suitable to use semi-log plot (Fig. 2).

**Table 1.** Superconductors and their parameters used in the work. In all calculations (except some original sources),  $\mu^* = 0.13$ .

Type / Chemical composition	$\lambda(0)$ (nm)	$\xi(0)$ (nm)	$\lambda_{\text{e-ph}}$	$T_c$ (K)	$T_\theta$ (K)	$\frac{2\Delta(0)}{k_B T_c}$	$T_F$ (10 <sup>3</sup> K)	$T_\theta/T_F$
<i>Pure metals</i>								
Aluminium				1.18 [58]	394 [5]		136 [5]	$2.9 \times 10^{-3}$
Aluminium	50 [57]	1550 [58]	0.43 [59]	1.18 [58]	394 [5]	3.535 [59]	18.9 (Eq. 12)	$2.1 \times 10^{-2}$
Tin				3.72 [58]	170 [5]		118 [5]	$1.4 \times 10^{-3}$
Tin	77 [60]	180 [58]	0.72 [59]	3.72 [58]	170 [5]	3.705 [59]	10.0 (Eq. 12)	$1.2 \times 10^{-2}$
Lead				7.20 [58]	88 [5]		110 [5]	$8 \times 10^{-4}$
Lead	64 [60]	87 [58]	1.55 [59]	7.20 [60]	88 [5]	4.497 [59]	11.2 (Eq. 12)	$7.8 \times 10^{-3}$
Niobium				9.25 [58]	265 [5]		61.8 [5]	$4.3 \times 10^{-3}$
Niobium	52 [58]	39 [58]	0.98 [59]	9.25 [58]	265 [5]	3.964 [59]	16.1 (Eq. 12)	$1.6 \times 10^{-2}$
<i>Al<sub>5</sub> Alloys</i>								
Nb <sub>3</sub> Sn	124 [61]	3.6 [61]	1.8 [62]	17.9 [61]	234 [61]	4.2 [62]	4.5 (Eq. 12)	$5.2 \times 10^{-2}$
V <sub>3</sub> Si	62 [62]	3.3 [62]	0.96 [62]	16.4 [62]	297 [64]	3.7 [62]	12.8 (Eq. 12)	$2.3 \times 10^{-2}$
Nb <sub>3</sub> Ge	90 [58]	3.0 [58]	1.60 [59]	23.2 [58]	302 [65]	4.364 [59]	7.1 (Eq. 12)	$4.3 \times 10^{-2}$
<i>Heusler alloys</i>								
ZrNi <sub>2</sub> Ga	350 [66]	15 [66]	0.551 [66]	2.85 [66]	300 [66]		1.4 (Eq. 12)	$2.2 \times 10^{-1}$
YPd <sub>2</sub> Sn	196 [67]	19 [67]	0.70 [67]	4.7 [67]	210 [67]	4.1 [67]	2.9 (Eq. 12)	$7.2 \times 10^{-2}$
HfPd <sub>2</sub> Al	225 [67]	13 [67]	0.68 [67]	3.66 [67]	182 [67]	3.74 [67]	2.4 (Eq. 12)	$7.5 \times 10^{-2}$
<i>Noncentrosymmetric</i>								
Nb <sub>0.5</sub> Os <sub>0.5</sub>	654 [68]	7.8 [68]	0.53 [68]	3.07 [68]	367 [68]	3.62 [68]	0.60 (Eq. 12)	$6.1 \times 10^{-1}$
Re <sub>6</sub> Zr (mSR)	356 [29]	3.7 [29]	0.67 [29]	6.75 [29]	338 [29]	3.72 [29]	1.3	$2.6 \times 10^{-1}$
Re <sub>6</sub> Zr (magnetization)	247 [29]	3.3 [29]	0.67 [29]	6.75 [29]	237 [29]	3.72 [29]	2.1	$1.1 \times 10^{-1}$
Mo <sub>3</sub> Al <sub>2</sub> C	376 [69]	4.2 [69]	(Eqs. 7-9)	9.2 [69]	339 [69]	4.03 [69]	1.2	$2.8 \times 10^{-1}$
NbIr <sub>2</sub> B <sub>2</sub> [70]	223	4.5	0.74	7.18	274		2.4	$1.1 \times 10^{-1}$
TaIr <sub>2</sub> B <sub>2</sub> [70]	342	4.7	0.70	5.1	230		1.4	$1.7 \times 10^{-1}$

$\text{Re}_3\text{Ta}$ [71]		0.62	4.7	321	0.64	5.0 $\times 10^{-1}$
<b>Laves phases</b>						
$\text{BaRh}_2$ [72]	340	8.4	0.80	5.6	178	1.4 $\times 10^{-1}$
$\text{SrRh}_2$ [72]	229	9.1	0.71	5.4	237	2.3 $\times 10^{-1}$
$\text{SrRh}_2$ [73]	121	8.6	0.93	5.4	250	5.3 $\times 10^{-2}$
$\text{SrIr}_2$ [74]	237	7.5	0.84	5.9	180	2.3 $\times 10^{-2}$
<b>Intermetallics</b>						
$\text{MgCNi}_3$ [75]	248	4.6	(Eqs. 7-9)	7.6	284	2.1 $\times 10^{-1}$
$\text{RuAl}_6$ [76]	265	27.7	0.81	1.21	458	1.9 $\times 10^{-1}$
<b>Perovskite</b>						
$\text{SrTiO}_3$		0.2 [7]	0.086 [8]	690 [77]	[8]	$1.3 \times 10^{-2}$ $5.3 \times 10^1$
<b>Pnictides</b>						
$\text{ThFeAsN}$	375 [78]	1.48 [78]	28.1 [78]	332 [79]	$0.47 \text{ (Eq. 15)}$ $c_{int} = 8.5 \text{ \AA} [78]$	$7.0 \times 10^{-1}$
$\text{KC}_{2\text{Fe}}\text{As}_4\text{F}_2$	230 [80]	1.59 [80]	33.4 [80]	366 [80]	$1.3 \text{ (Eq. 15)}$ $c_{int} = 8.5 \text{ \AA} [80]$	$2.9 \times 10^{-1}$
$\text{RbCa}_2\text{Fe}_4\text{As}_4\text{F}_2$	232 [80]	1.45 [80]	29.2 [80]	332 [80]	$1.2 \text{ (Eq. 15)}$ $c_{int} = 8.5 \text{ \AA} [80]$	$2.8 \times 10^{-1}$
$\text{CsCa}_2\text{Fe}_4\text{As}_4\text{F}_2$	244 [80]	1.44 [80]	28.3 [80]	344 [80]	$1.1 \text{ (Eq. 15)}$ $c_{int} = 8.5 \text{ \AA} [80]$	$3.1 \times 10^{-1}$
<b>Cuprates</b>						
$\text{YBa}_2\text{Cu}_3\text{O}_7$ [81]	115 [81,82]	2.5 [81]	1.5 [83]	93.2 [81]	437 [7]	$3.4 \text{ (Eq. 15)}$ $c_{int} = 5.8 \text{ \AA} [83]$
$(\text{Y},\text{Dy})\text{Ba}_2\text{Cu}_3\text{O}_7$ [88]	128 [88,89]	2.5 [81]	1.5 [83]	90.4 [88,89]	437 [7]	$2.9 \text{ (Eq. 15)}$ $c_{int} = 5.8 \text{ \AA} [83]$
$\text{Bi}_2\text{Sr}_2\text{CaCu}_2\text{O}_8$ [90]	196 [89]	1.2 [89]	4.7 [7]	82.7 [89]	240 [7]	$1.2 \text{ (Eq. 15)}$ $c_{int} = 6 \text{ \AA} [83]$
$\text{Tl}_2\text{Ba}_2\text{CaCu}_2\text{O}_8$ [91]	179 [89]	1.2 [89]		103 [89]	425 [87]	$1.5 \text{ (Eq. 15)}$ $c_{int} = 6 \text{ \AA} [83]$
$\text{HgBa}_2\text{CaCu}_2\text{O}_8$ [92]	188 [89]	1.6 [89]		120 [89]	525 [87]	$1.3 \text{ (Eq. 15)}$ $c_{int} = 6 \text{ \AA} [83]$
$\text{Bi}_2\text{Sr}_2\text{Ca}_2\text{Cu}_3\text{O}_{10}$ [93]	175 [89]	1.0 [89]	4.5	85 [89]	319 [7]	$1.5 \text{ (Eq. 15)}$ $c_{int} = 6 \text{ \AA} [83]$

<b>Twisted graphene</b>						
MATBG [94]	2180 [95]	$\frac{m^*}{m_e} = 0.2$ [95]	1.2 [95]	1864 [96]	4.4 [95]	$16.5 \times 10^{-3}$ (Eq. 15) $c_{int} = 1 \text{ nm}$ $1.1 \times 10^2$
MATBG [94]	61.4 [95]	$\frac{m^*}{m_e} = 0.2$ [95]	1.2 [95]	1864 [96]	4.4 [95]	$28.6 \times 10^{-3}$ (Eq. 16) $6.5 \times 10^1$
<b>Ionic Salt</b>						
CsI ( $P = 206 \text{ GPa}$ ) [97]		0.445 [98]	1.1 [97]	339 [98]	$(20 \pm 4) \times 10^{-2}$ [98]	$17 \pm 4$ [98]
<b>NRTS hydrides</b>						
H <sub>3</sub> S ( $P = 155 \text{ GPa}$ ) [54]	37 [52]	1.9 [54]	2.2 [99]	197 [99]	1427 [99]	$21.6$ (Eq. 12) $6.6 \times 10^{-2}$
H <sub>3</sub> S ( $P = 155 \text{ GPa}$ ) [54]		1.86 [100]	1.76 [55,56,100]	190 [100]	1427 [99]	$6$ [100] $(2.4) \times 10^{-1}$ (Eq. 16)
H <sub>3</sub> S ( $P = 155 \text{ GPa}$ ) [54]		1.92 [100]	1.76 [55,56,100]	188 [100]	1427 [99]	$5$ [100] $(\text{Eq. 16})$ $2.9 \times 10^{-1}$
H <sub>3</sub> S ( $P = 160 \text{ GPa}$ ) [54]		2.18 [100]	1.76 [55,56,100]	171 [100]	1427 [99]	$10.7$ [100] $(\text{Eq. 16})$ $1.3 \times 10^{-1}$
H <sub>3</sub> S ( $P = 160 \text{ GPa}$ ) [54]		2.67 [100]	1.76 [55,56,100]	150 [100]	1427 [99]	$10.1$ [100] $(\text{Eq. 16})$ $1.4 \times 10^{-1}$
LaH <sub>10</sub> ( $P = 150 \text{ GPa}$ ) [36]	30 [51]		2.77 [27]	240 [27]	1310 [27]	$27.0$ (Eq. 12) $2.7 \times 10^{-2}$
LaH <sub>10</sub> ( $P = 150 \text{ GPa}$ ) [36]		1.5 [51]	2.77 [27]	240 [27]	1310 [27]	$3.53$ [assumed] $8.5$ (Eq. 16) $1.5 \times 10^{-1}$
LaH <sub>10</sub> ( $P = 150 \text{ GPa}$ ) [36]		1.5 [51]	2.77 [27]	240 [27]	1310 [27]	$5.0$ [assumed] $17.0$ (Eq. 12) $7.7 \times 10^{-2}$
La <sub>1-x</sub> Nd <sub>x</sub> H <sub>10</sub> ( $x=0.15$ ) ( $P = 180 \text{ GPa}$ ) [48]		2.3 [101]	1.65 [101]	122 [101]	1156 [101]	$4.4$ [101] $(\text{Eq. 16})$ $2.6 \times 10^{-1}$
<b>Compressed oxygen</b>						
$\zeta$ -O <sub>2</sub> ( $P=115 \text{ GPa}$ ) [102]		42 [103]	0.42 [103]	0.64 [103]	306 [103]	$3.5 \times 10^{-2}$ [103] (Eq. 16) 8.7

And finally in Figure 3 we represented same superconducting materials, but here we displayed  $T_c$  vs  $\frac{T_\theta}{T_F}$  dataset in log-log plot. This type of plot was chosen because as  $T_c$ , as  $\frac{T_\theta}{T_F}$  are varied within several orders of magnitude.

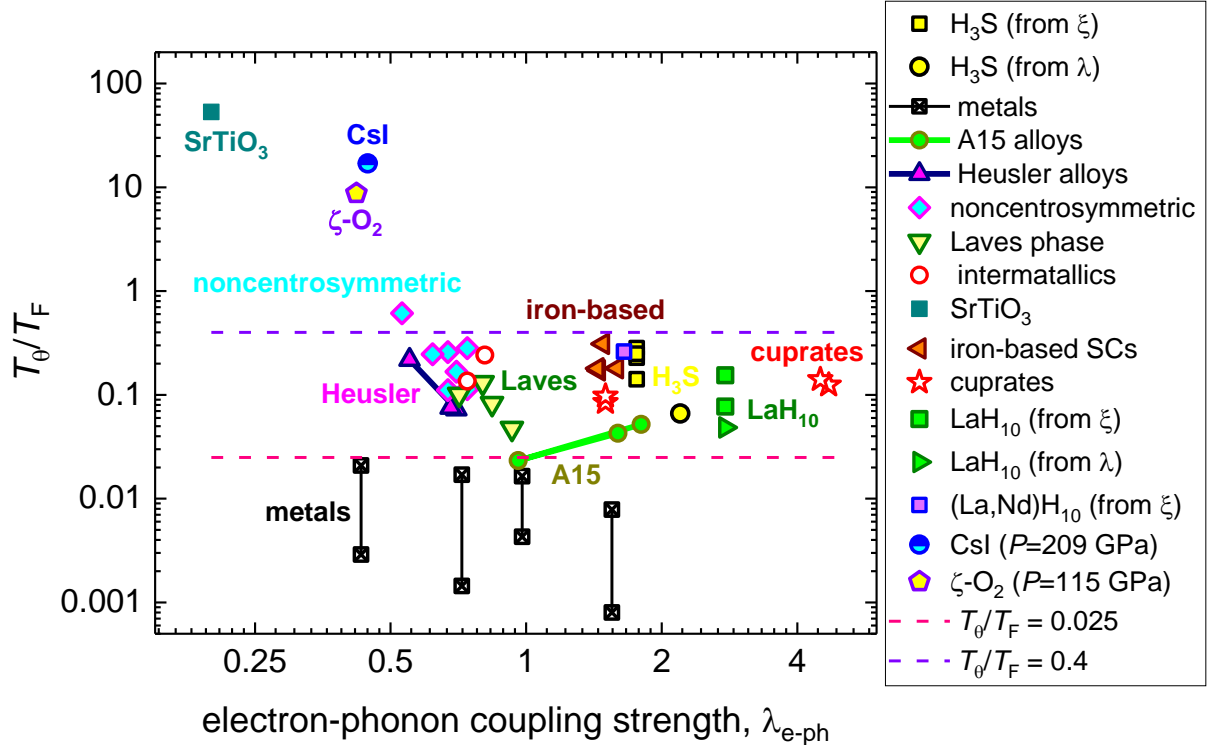


**Figure 2.** Plot of  $\frac{T_\theta}{T_F}$  vs  $\lambda_{e-ph}$  for primary superconducting families. This type of plot proposed by Pietronero *et al* [13]. References on original data ( $T_\theta$ ,  $\lambda_{e-ph}$ ,  $T_F$ ) can be found in Table 1.

#### 4. Discussion

The family of near-room temperature superconductors (NRTS) is represented in Table SI and Fig. 1 by  $H_3S$  ( $P = 155,160$  GPa),  $LaH_{10}$  ( $P = 150$  GPa) and  $La_{1-x}Nd_xH_{10}$  ( $x = 0.09$ ,  $P = 180$  GPa). Two different approaches to calculate  $T_F$  in NRTS materials were used:

1.  $T_F$  was calculated based on Eqs. 12,13. In these calculations  $\lambda(0) = 37$  nm (extracted from the analysis of DC magnetization experiments reported by Minkov *et al* [51,52]) was used. By doing this, we used “classical” approach implemented by Uemura [18] to calculate the Fermi temperature,  $T_F$ , in cuprates from ground state London penetration depth,  $\lambda(0)$ . Data points derived by this approach designated in Figures 1-3 by “from  $\lambda$  ”.
2.  $T_F$  was calculated based Eqs. 6-9,18, in which utilized  $\xi(0)$  values. Data points derived by this approach designated in Figures 1-3 by “from  $\xi$  ”.

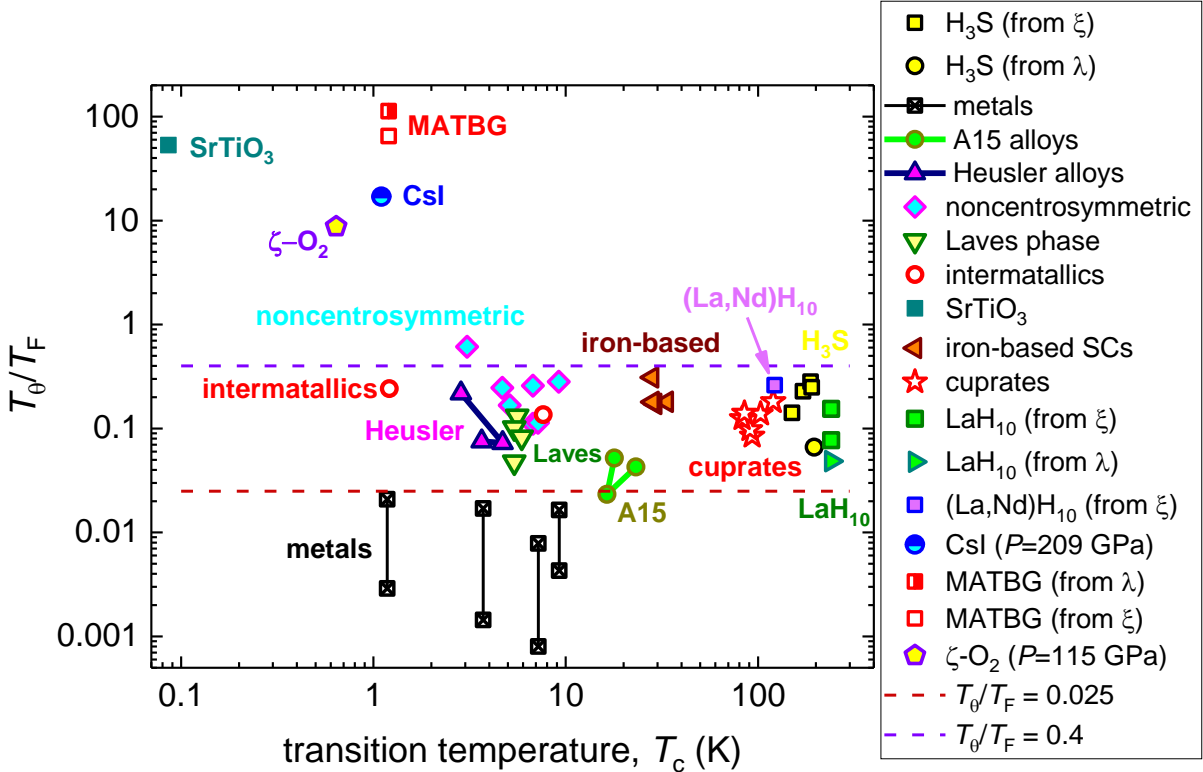


**Figure 3.** Plot  $\frac{T_\theta}{T_F}$  vs  $T_c$  for primary superconducting families. References on original data ( $T_\theta$ ,  $T_c$ ,  $T_F$ ) can be found in Table 1.

It should be noted that in both approaches the electron-phonon coupling strength constant,  $\lambda_{e-ph}$ , was assumed to be  $\lambda_{e-ph} = 1.76$ , which is averaged value of values calculated by first-principles calculations [55,56] and values extracted from experimental  $R(T)$  data [27].

It can be seen in Table 1 and Fig. 1, that calculated  $T_F$  values for  $H_3S$  by two alternative approaches are in a very good agreement with each other. To demonstrate the acceptable level of variation in  $T_F$  values for the same material, in Table 1 and Fig. 1 we presented results of calculations for pure metals, where  $T_F$  was calculated by two mentioned above approaches and the use of experimental data reported by different research groups.

Excluding the  $YBa_2Cu_3O_{7-x}$ , the  $T_F$  in HTS cuprates were calculated based on the effective electron-phonon coupling constants,  $\lambda_{e-ph,eff}$ , reported by Ledbetter *et al* [7], from which the effective mass can be deduced,  $m^* = (1 + \lambda_{e-ph,eff}) \times m_e$ .

For  $\text{YBa}_2\text{Cu}_3\text{O}_7$  (for the purpose of consistency with works by Uemura [83]) we used the relation [83]:

$$\frac{m^*}{m_e} = 2.5 \quad (17)$$

from which  $\lambda_{e-ph} = 1.5$  can be derived. Proposed values are in a reasonable agreement with experimental  $\frac{m^*}{m_e}$  values reported by several research groups [84-86] in  $\text{YBa}_2\text{Cu}_3\text{O}_{7-x}$ . For calculations we used the Debye temperature in cuprates reported by Ledbetter *et al* [7,87].

It should be mention the result of  $T_F$  calculation in MATBG (Table 1),  $T_F = 16.5 \text{ K}$ , which was primarily based on the London penetration depth,  $\lambda(0) = 1860 \text{ nm}$ , deduced in Ref. 95 from the self-field critical current density,  $J_c(sf, T)$ , by the approach proposed by us [88]:

$$J_c(sf, T) = \frac{\phi_0}{4\pi\mu_0} \frac{\ln(1+\sqrt{2}\kappa(T))}{\lambda^3(T)} \quad (18)$$

Remarkable agreement of the deduced value,  $T_F = 16.5 \text{ K}$ , and the value reported in original work on MATBG by Cao *et al* [94],  $T_F = 17 \text{ K}$ , which was calculated based on normal state charge carriers density in MATBG, independently validates our primary idea [88] about fundamental nature of the self-field critical current in weak-links samples [88,89,104]. Recent prove of this concept has reported by Paturi and Huhtinen [105] who utilized a fact that the London penetration depth,  $\lambda(0)$ , in real samples depends from the mean free-path of charge carriers,  $l$ :

$$\lambda(0) = \lambda_{clean\ limit}(0) \sqrt{1 + \frac{\xi(0)}{l}} \quad (19)$$

where  $\lambda(0)$  is effective penetration depth, and  $\lambda_{clean\ limit}(0)$  is the penetration depth in samples exhibits very long mean free-path,  $l \gg \xi(0)$ . Paturi and Huhtinen [105] varied  $l$  in  $\text{YBa}_2\text{Cu}_3\text{O}_{7-x}$  films and showed that the change in  $J_c(st, T)$  satisfies with Eqs. 18,19.

The MATBG does not show in the Figure 2, because the derivation of  $\lambda_{e-ph}$  cannot be performed by the used phenomenology:  $m^* = (1 + \lambda_{e-ph}) \times m_e$ , because  $\frac{m^*}{m_e} = 0.2$  [95], however, this material is shown in Figures 1,3, because  $\lambda_{e-ph}$  is not required for these plots.

Returning back to hydrides, we need to note, that Durajski [56] performed first-principles studies on the strength of nonadiabatic effects in highly-compressed sulphur hydride and phosphorus hydride. Calculations [56] showed that the strength of the nonadiabatic effects in these hydrides can be quantify as moderate in comparison with classical nonadiabatic superconductors, like  $\text{SrTiO}_3$ . This is in a good agreement with our result (see Figure 3 and Table 1) that all deduced  $\frac{T_\theta}{T_F}$  values for NRTS are within the range of:

$$0.03 \leq \frac{T_\theta}{T_F} \leq 0.3. \quad (20)$$

Considering primary difference between Figs. 1-3, we need to mention that very strong nonadiabatic superconductors (i.e. MATBG, CsI, and  $\zeta\text{-O}_2$ ) in the Uemura plot (Fig. 1) are located inside of the unconventional superconductors band  $0.01 \leq \frac{T_c}{T_F} \leq 0.05$  which is not a clear way to manifest primary unique property of this materials, because pnictides, cuprates, and hydrides are also located in the same band.

Moreover, classical nonadiabatic superconductor  $\text{SrTiO}_3$  falls in intermediate zone between unconventional and BCS superconductors, because for this material exhibits  $\frac{T_c}{T_F} = 0.0066$ , and by this criterion,  $\text{SrTiO}_3$  is similar to the Laves phase materials, intermetallics, A-15 alloys, and Heusler alloys, which cannot be considered to be correct manifestation of primary uniqueness of this materials which is nonadiabaticity.

However, in Figs. 2 and 3, the outstanding separations of all nonadiabatic superconductors from its adiabatic and moderate nonadiabatic counterparts is clearly manifested.

By looking at the data in Figures 2 and 3, it is easy to recognize that ¾ (30 of 40) of analysed superconductors fall into reasonably narrow band:

$$0.025 \leq \frac{T_\theta}{T_F} \leq 0.4 \quad (21)$$

despite a fact, that no any selectivity criterion was applied to include data in the databased.

Based on this, we proposed to use the values in the Eq. 21 as empirical limits for the adiabatic superconductors ( $\frac{T_\theta}{T_F} \leq 0.025$ ), moderate nonadiabatic superconductors ( $0.025 \leq \frac{T_\theta}{T_F} \leq 0.4$ ), and strong nonadiabatic superconductors ( $\frac{T_\theta}{T_F} \geq 0.4$ ).

As it follows from our analysis that all strong nonadiabatic superconductors exhibits low superconducting transition temperatures,  $T_c \leq 1.2 K$  (Fig. 3).

It should be mentioned that Hirsch and Marsiglio in series of papers [106-109] claimed the absence of the superconductivity as a physical phenomenon in highly-compressed hydrides. In one occasion [110], we already showed that one their claims [109] is incorrect.

It is important to stress, that in 2015 Hirsch and Marsiglio [111] completely supported the discovery of the superconductivity in  $H_3S$  and extended their theory of hole superconductivity [112-114] on  $H_3S$  and “other sulphates” [111]. In overall, Hirsch and Marsiglio theory of hole superconductivity [112-114] is (not exactly, but roughly speaking) based on an idea that “only hole conductors can be superconductors” [114].

In following years (after 2015), Hirsch and Marsiglio published several papers [115-117], where in regard of  $H_3S$ , Souza and Marsiglio stated: “...We find high critical temperatures are possible, even with very modest coupling strengths. ...” [116].

More clearly the statement had expressed by Hirsch [117] in 2017:  
*“... In addition, we have argued [...] that these models lead to hole pairing and superconductivity in the following classes [...] of superconducting materials:*

*(1) Hole-doped cuprates [...]*

- (2) *Electron-doped cuprates [...]*
- (3) *Magnesium diboride [...]*
- (4) *Transition metal series alloys [...]*
- (5) *Iron pnictides [...]*
- (6) *Iron selenides [...]*
- (7) *Doped semiconductors [...]*
- (8) *Elements under high pressure [...]*
- (9) *Sulphur hydride [...]*
- (10) *A-15 materials [...]*
- (11) *All other superconductors [...]”.*

All claims by Hirsch and Marsiglio [106-109] about the absence of the phenomenon of the superconductivity in hydrides have a very sharp starting time, which is the publication of experimental data by Mozafarri *et al* [54] who showed that the H<sub>3</sub>S is the electron-type conductor.

Due to, in overall, Hirsch and Marsiglio theory of hole superconductivity [112-114] is in a strike disagreement with experimental data on cuprates and pnictides [118], and, even, on SrTiO<sub>3</sub> (Table 1) (which is *n*-type semiconductor [8]), that eventually all claims by Hirsch and Marsiglio [106-109] about the absence of superconductivity in hydrides will be answered based on scientific background. However, the Brandolini's law [119] is directly applied to the efforts to refute statements expressed by these authors.

## **5. Conclusions**

In this work we proposed a new calcification scheme to quantify the effects of nonadiabaticity in superconductors. By performing the analysis of experimental data for 40 superconductors, which represent primary families of superconductors, we found that ¾ of all

analysed superconductors falls into narrow  $0.025 \leq \frac{T_\theta}{T_F} \leq 0.4$  band. Based on this, we proposed the taxonomy for the strength of the nonadiabatic effects in superconductors.

## Acknowledgments

The author thanks Luciano Pietronero (Universita' di Roma) for explanations of the limitations of the Bardeen-Cooper-Schrieffer (BCS) and Migdal–Eliashberg (ME) theories of electron–phonon-mediated superconductivity.

## References

1. Bardeen, J.; Cooper, L.N.; Schrieffer, J.R. Theory of superconductivity. *Phys. Rev.* **1957**, *108*, 1175–1204. 10.1103/PhysRev.108.1175.
2. Migdal, A.B. Interaction between electrons and lattice vibrations in a normal metal. *Sov. Phys. JETP* **1958**, *7*, 996–1001.
3. Eliashberg, G.M. Interactions between electrons and lattice vibrations in a superconductor. *Sov. Phys. JETP* **1960**, *11*, 696–702.
4. Pietronero, L.; Strässler, S.; Grimaldi, C. Nonadiabatic superconductivity. I. Vertex corrections for the electron-phonon interactions. *Phys. Rev. B* **1995**, *52*, 10516–10529. 10.1103/PhysRevB.52.10516.
5. Poole, C.P., Jr. Properties of the normal metallic state. In *Handbook of Superconductivity*, 1st ed.; Poole, C.P., Jr., Ed.; Academic Press: New York, NY, USA, 1999; pp. 31–32.
6. Takada, Y. Theory of superconductivity in polar semiconductors and its application to n-type semiconducting SrTiO<sub>3</sub>. *J. Phys. Soc. Jpn.* **1980**, *49*, 1267–1275. 10.1143/JPSJ.49.1267
7. Ledbetter, H.; Lei, M.; Kim, S. Elastic constants, Debye temperatures, and electron-phonon parameters of superconducting cuprates and related oxides. *Phase Transitions* **1990**, *23*, 61–70. 10.1080/01411599008241819.
8. Lin, X.; Zhu, Z.; Fauque, B.; Behnia, K. Fermi surface of the most dilute superconductor. *Physical Review X* **2013**, *3*, 021002. 10.1103/PhysRevX.3.021002.
9. Takada, Y. Plasmon mechanism of superconductivity in two- and three-dimensional electron systems. *J. Phys. Soc. Jpn.* **1978**, *45*, 786–794. 10.1143/JPSJ.45.786
10. Grimaldi, C.; Pietronero, L.; Strässler, S. Nonadiabatic superconductivity. II. Generalized Eliashberg equations beyond Migdal's theorem. *Phys. Rev. B* **1995**, *52*, 10530–10546. <https://doi.org/10.1103/PhysRevB.52.10530>.
11. Grimaldi, C.; Cappelluti, E.; Pietronero, L. Isotope effect on  $m^*$  in high  $T_c$  materials due to the breakdown of Migdal's theorem. *Europhys. Lett.* **1998**, *42*, 667–672. 10.1209/epl/i1998-00303-0.
12. Cappelluti, E.; Ciuchi, S.; Grimaldi, C.; Pietronero, L.; Strässler, S. High  $T_c$  superconductivity in MgB<sub>2</sub> by nonadiabatic pairing. *Phys. Rev. Lett.* **2002**, *88*, 117003. 10.1103/PhysRevLett.88.117003.
13. Pietronero, L.; Boeri, L.; Cappelluti, E.; Ortenzi, L. Conventional/unconventional superconductivity in high-pressure hydrides and beyond: Insights from theory and perspectives. *Quantum Stud. Math. Found.* **2018**, *5*, 5–21. 10.1007/s40509-017-0128-8.
14. Klimin, S.N.; Tempere, J.; Devreese, J. T.; He, J.; Franchini, C.; Kresse, G. Superconductivity in SrTiO<sub>3</sub>: Dielectric function method for non-parabolic bands. *Journal of Superconductivity and Novel Magnetism* **2019**, *32*, 2739–2744. 10.1007/s10948-019-5029-0.
15. Gor'kov, L.P. Phonon mechanism in the most dilute superconductor n-type SrTiO<sub>3</sub>. *PNAS* **2016**, *113*, 4646–4651. 10.1073/pnas.1604145113.
16. Kresin, V. Z.; and Wolf, S. A. *Colloquium: Electron-lattice interaction and its impact on high  $T_c$  superconductivity*. *Review of Modern Physics* **2009**, *81*, 481–501. 10.1103/RevModPhys.81.481.
17. Harshman, R.; Fiory, A. T. High- $T_c$  superconductivity in hydrogen clathrates mediated by Coulomb interactions between hydrogen and central-atom electrons. *J. Supercond. Novel Magn.* **2020**, *33*, 2945–2961. 10.1007/s10948-020-05557-4.

18. Uemura, Y. J. Classifying superconductors in a plot of  $T_c$  versus Fermi temperature  $T_F$ . *Physica C* **1991**, *185–189*, 733–734. 10.1016/S0921-4534(97)00194-9.
19. Talantsev, E.F.; Crump, W.P.; Tallon, J.L. Universal scaling of the self-field critical current in superconductors: From sub-nanometre to millimetre size. *Sci. Rep.* **2017**, *7*, 10010. 10.1038/s41598-017-10226-z.
20. Homes, C. C.; Dordevic, S. V.; Strongin, M.; Bonn, D. A.; Liang, R.; Hardy, W. N.; Komiya, S.; Ando, Y.; Yu, G.; Kaneko, N.; et al. A universal scaling relation in high-temperature superconductors. *Nature* **2004**, *430*, 539–541. 10.1038/nature02673.
21. Koblischka, R.; Koblischka-Veneva, A. Calculation of  $T_c$  of superconducting elements with the Roeser–Huber formalism. *Metals* **2022**, *12*, 337. 10.3390/met12020337.
22. Zhang, T.; Jiang, Y.; Song, Z.; Huang, H.; He, Y.; Fang, Z.; Weng, H.; Fang, C. Catalogue of topological electronic materials. *Nature* **2019**, *566*, 475–479. 10.1038/s41586-019-0944-6.
23. Xu, Y.; Vergniory, M. G.; Ma, D.-S.; Mañes, J. L.; Song, Z.-D.; Bernevig, B. A.; Regnault, N.; Elcoro, L. Catalogue of topological phonon materials. *arXiv* **2022**, *2211.11776*. 10.48550/arXiv.2211.11776.
24. Pyon, S.; Kudo, K.; Matsumura, J.-I.; Ishii, H.; Matsuo, G.; Nohara, M.; Hojo, H.; Oka, K.; Azuma, M.; Garlea, V.O.; et al. Superconductivity in noncentrosymmetric iridium silicide  $\text{Li}_2\text{IrSi}_3$ . *J. Phys. Soc. Jpn.* **2014**, *83*, 093706. 10.7566/JPSJ.83.093706.
25. Kudo, K.; Hiiragi, H.; Honda, T.; Fujimura, K.; Idei, H.; Nohara, M. Superconductivity in  $\text{Mg}_2\text{Ir}_3\text{Si}$ : A fully ordered Laves phase. *J. Phys. Soc. Jpn.* **2020**, *89*, 013701. 10.7566/JPSJ.89.013701.
26. Sobczak, Z.; Winiarski, M. J.; Xie, W.; Cava, R. J.; Klimczuk, T. Superconductivity in the intermetallic compound  $\text{Zr}_5\text{Al}_4$ . *EPL* **2019**, *127*, 37005. 10.1209/0295-5075/127/37005.
27. Talantsev, E.F. Advanced McMillan's equation and its application for the analysis of highly-compressed superconductors. *Supercond. Sci. Technol.* **2020**, *33*, 094009. 10.1088/1361-6668/ab953f.
28. Talantsev, E.F. The electron–phonon coupling constant and the Debye temperature in polyhydrides of thorium, hexadeuteride of yttrium, and metallic hydrogen phase III. *J. Appl. Phys.* **2021**, *130*, 195901. 10.1063/5.0065003.
29. Mayoh, D. A.; Barker, J. A. T.; Singh, R. P.; Balakrishnan, G.; Paul, D. McK.; Lees, M. R. Superconducting and normal-state properties of the noncentrosymmetric superconductor  $\text{Re}_6\text{Zr}$ . *Phys. Rev. B* **2017**, *96*, 064521. 10.1103/PhysRevB.96.064521.
30. McMillan, W.L. Transition temperature of strong-coupled superconductors. *Phys. Rev.* **1968**, *167*, 331–344. <https://doi.org/10.1103/PhysRev.167.331>.
31. Vignolle, B.; Vignolles, D.; LeBoeuf, D.; Lepault, S.; Ramshaw, B.; Liang, R.; Bonn, D. A.; Hardy, W. N.; Doiron-Leyraud, N.; Carrington, A.; et al. Quantum oscillations and the Fermi surface of high-temperature cuprate superconductors. *Comptes Rendus Physique* **2011**, *12*, 446–460. 10.1016/j.crhy.2011.04.011.
32. Poole, C.P., Jr. Properties of the normal metallic state. In *Handbook of Superconductivity*, 1st ed.; Poole, C.P., Jr., Ed.; Academic Press: New York, NY, USA, 1999; Volume 1, pp. 36–38.
33. Poole, C.P., Jr. Properties of the normal metallic state. In *Handbook of Superconductivity*, 1st ed.; Poole, C.P., Jr., Ed.; Academic Press: New York, NY, USA, 1999; pp. 53–60.
34. Talantsev, E. F. Critical de Broglie wavelength in superconductors. *Mod. Phys. Lett. B* **2018**, *32*, 1850114. 10.1142/S0217984918501142.
35. Drozdov, A.P.; Eremets, M.I.; Troyan, I.A.; Ksenofontov, V.; Shylin, S.I. Conventional superconductivity at 203 kelvin at high pressures in the sulfur hydride system. *Nature* **2015**, *525*, 73–76. <https://doi.org/10.1038/nature14964>.
36. Drozdov, A.P.; Kong, P.P.; Minkov, V.S.; Besedin, S.P.; Kuzovnikov, M.A.; Mozaffari, S.; Balicas, L.; Balakirev, F.F.; Graf, D.E.; Prakapenka, V.B.; et al. Superconductivity at 250 K in lanthanum hydride under high pressures. *Nature* **2019**, *569*, 528–531. 10.1038/s41586-019-1201-8.
37. Somayazulu, M.; Ahart, M.; Mishra, A.K.; Geballe, Z.M.; Baldini, M.; Meng, Y.; Struzhkin, V.V.; Hemley, R.J. Evidence for superconductivity above 260 K in lanthanum superhydride at megabar pressures. *Phys. Rev. Lett.* **2019**, *122*, 027001. <https://doi.org/10.1103/PhysRevLett.122.027001>.
38. Semenok, D.V.; Kvashnin, A.G.; Ivanova, A.G.; Svitlyk, V.; Fominski, V.Y.; Sadakov, A.V.; Sobolevskiy, O.A.; Pudalov, V.M.; Troyan, I.A.; Oganov, A.R. Superconductivity at 161 K in thorium hydride  $\text{ThH}_{10}$ : Synthesis and properties. *Mater. Today* **2020**, *33*, 36–44. <https://doi.org/10.1016/j.mattod.2019.10.005>.
39. Chen, W.; Semenok, D.V.; Kvashnin, A.G.; Huang, X.; Kruglov, I.A.; Galasso, M.; Song, H.; Duan, D.; Goncharov, A.F.; Prakapenka, V.B.; et al. Synthesis of molecular metallic barium superhydride: Pseudocubic  $\text{BaH}_{12}$ . *Nat. Commun.* **2021**, *12*, 273. <https://doi.org/10.1038/s41467-020-20103-5>.
40. Troyan, I.A.; Semenok, D.V.; Kvashnin, A.G.; Sadakov, A.V.; Sobolevskiy, O.A.; Pudalov, V.M.; Ivanova, A.G.; Prakapenka, V.B.; Greenberg, E.; Gavriliuk, A.G.; et al. Anomalous high-temperature superconductivity in  $\text{YH}_6$ . *Adv. Mater.* **2021**, *33*, 2006832. <https://doi.org/10.1002/adma.202006832>.
41. Kong, P.; Minkov, V.S.; Kuzovnikov, M.A.; Drozdov, A.P.; Besedin, S.P.; Mozaffari, S.; Balicas, L.; Balakirev, F.F.; Prakapenka, V.B.; Chariton, S.; et al. Superconductivity up to 243 K in yttrium hydrides under high pressure. *Nat. Commun.* **2021**, *12*, 5075. <https://doi.org/10.1038/s41467-021-25372-2>.

42. Ma, L.; Wang, K.; Xie, Y.; Yang, X.; Wang, Y.; Zhou, M.; Liu, H.; Yu, X.; Zhao, Y.; Wang, H.; et al. High-temperature superconducting phase in clathrate calcium hydride  $\text{CaH}_6$  up to 215 K at a pressure of 172 GPa. *Phys. Rev. Lett.* **2022**, *128*, 167001. <https://doi.org/10.1103/PhysRevLett.128.167001>.
43. Semenok, D.V.; Troyan, I.A.; Ivanova, A.G.; Kvashnin, A.G.; Kruglov, I.A.; Hanfland, M.; Sadakov, A.V.; Sobolevskiy, O.A.; Pervakov, K.S.; Lyubutin, I.S.; et al. Superconductivity at 253 K in lanthanum–yttrium ternary hydrides. *Mater. Today* **2021**, *48*, 18–28. <https://doi.org/10.1016/j.mattod.2021.03.025>.
44. Zhou, D.; Semenok, D.V.; Duan, D.; Xie, H.; Chen, W.; Huang, X.; Li, X.; Liu, B.; Oganov, A.R.; Cui, T. Superconducting praseodymium superhydrides. *Sci. Adv.* **2020**, *6*, eaax6849. <https://doi.org/10.1126/sciadv.aax6849>.
45. Hong, F.; Shan, P.F.; Yang, L.X.; Yue, B.B.; Yang, P.T.; Liua, Z.Y.; Sun, J.P.; Dai, J.H.; Yu, H.; Yin, Y.Y.; et al. Possible superconductivity at ~70 K in tin hydride  $\text{SnH}_x$  under high pressure. *Mater. Today Phys.* **2022**, *22*, 100596. [10.1016/j.mtphys.2021.100596](https://doi.org/10.1016/j.mtphys.2021.100596).
46. Chen, W.; Semenok, D.V.; Huang, X.; Shu, H.; Li, X.; Duan, D.; Cui, T.; Oganov, A.R. High-temperature superconducting phases in cerium superhydride with a  $T_c$  up to 115 K below a pressure of 1 Megabar. *Phys. Rev. Lett.* **2021**, *127*, 117001. [10.1103/PhysRevLett.127.117001](https://doi.org/10.1103/PhysRevLett.127.117001).
47. Osmond, I.; Moulding, O.; Cross, S.; Muramatsu, T.; Brooks, A.; Lord, O.; Fedotenko, T.; Buhot, J.; Friedemann, S. Clean-limit superconductivity in  $\text{Im}3m$   $\text{H}_3\text{S}$  synthesized from sulfur and hydrogen donor ammonia borane. *Phys. Rev. B* **2022**, *105*, L220502. [10.1103/physrevb.105.l220502](https://doi.org/10.1103/physrevb.105.l220502).
48. Semenok, D.V.; Troyan, I.A.; Sadakov, A.V.; Zhou, D.; Galasso, M.; Kvashnin, A.G.; Ivanova, A.G.; Kruglov, I.A.; Bykov, A.A.; Terent'ev, K.Y.; et al. Effect of magnetic impurities on superconductivity in  $\text{LaH}_{10}$ . *Adv. Mater.* **2022**, *34*, 2204038. [10.1002/adma.202204038](https://doi.org/10.1002/adma.202204038).
49. Bi, J.; Nakamoto, Y.; Zhang, P.; Shimizu, K.; Zou, B.; Liu, H.; Zhou, M.; Liu, G.; Wang, H.; Ma, Y. Giant enhancement of superconducting critical temperature in substitutional alloy  $(\text{La},\text{Ce})\text{H}_9$ . *Nature Communications* **2022**, *13*, 5952. [10.1038/s41467-022-33743-6](https://doi.org/10.1038/s41467-022-33743-6).
50. Li, Z.; He, X.; Zhang, C.; Wang, X.; Zhang, S.; Jia, Y.; Feng, S.; Lu, K.; Zhao, J.; Zhang, J.; et al. Superconductivity above 200 K discovered in superhydrides of calcium. *Nat. Commun.* **2022**, *13*, 2863. [10.1038/s41467-022-30454-w](https://doi.org/10.1038/s41467-022-30454-w).
51. Minkov, V. S.; Bud'ko, S. L.; Balakirev, F. F.; Prakapenka, V. B.; Chariton, S.; Husband, R. J.; Liermann, H. P.; Eremets, M. I. Magnetic field screening in hydrogen-rich high-temperature superconductors. *Nature Communications* **2022**, *13*, 3194. [10.1038/s41467-022-30782-x](https://doi.org/10.1038/s41467-022-30782-x).
52. Minkov, V. S.; Ksenofontov, V.; Budko, S. L.; Talantsev, E. F.; Eremets, M. I. Trapped magnetic flux in hydrogen-rich high-temperature superconductors. *arXiv* **2022**, *arXiv:2206.14108*. [10.48550/arXiv.2206.14108](https://doi.org/10.48550/arXiv.2206.14108).
53. Talantsev, E.F. Classifying superconductivity in compressed  $\text{H}_3\text{S}$ . *Mod. Phys. Lett. B* **2019**, *33*, 1950195. [10.1142/S0217984919501951](https://doi.org/10.1142/S0217984919501951).
54. Mozaffari, S.; Sun, D.; Minkov, V.S.; Drozdov, A.P.; Knyazev, D.; Betts, J.B.; Einaga, M.; Shimizu, K.; Eremets, M.I.; Balicas, L. Superconducting phase-diagram of  $\text{H}_3\text{S}$  under high magnetic fields. *Nat. Commun.* **2019**, *10*, 2522. [10.1038/s41467-019-10552-y](https://doi.org/10.1038/s41467-019-10552-y).
55. Errea, I.; Calandra, M.; Pickard, C. J.; Nelson, J.; Needs, R. J.; Li, Y.; Liu, H.; Zhang, Y.; Ma, Y.; Mauri, F. High-pressure hydrogen sulfide from first principles: A strongly anharmonic phonon-mediated superconductor. *Phys. Rev. Lett.* **2015**, *856*, 1–78.
56. Durajski, A. P. Quantitative analysis of nonadiabatic effects in dense  $\text{H}_3\text{S}$  and  $\text{PH}_3$  superconductors. *Sci Rep* **2016**, *6*, 38570. [10.1038/srep38570](https://doi.org/10.1038/srep38570).
57. Prozorov, R.; Giannetta, R. W.; Carrington, A.; Fournier, P.; Greene, R. L.; Guptasarma, P.; Hinks, D. G.; Banks, A. R. Measurements of the absolute value of the penetration depth in high- $T_c$  superconductors using a low- $T_c$  superconductive coating. *Appl. Phys. Lett.* **2000**, *77*, 4202–4204. [10.1063/1.1328362](https://doi.org/10.1063/1.1328362).
58. Poole, C.P., Jr. Properties of the normal metallic state. In *Handbook of Superconductivity*, 1st ed.; Poole, C.P., Jr., Ed.; Academic Press: New York, NY, USA, 1999; pp. 433–445.
59. Carbotte, J.P. Properties of boson-exchange superconductors. *Rev. Mod. Phys.* **1990**, *62*, 1027–1157. [10.1103/RevModPhys.62.1027](https://doi.org/10.1103/RevModPhys.62.1027).
60. Peabody, G.E.; Meservey, R. Magnetic flux penetration into superconducting thin films. *Phys. Rev. B* **1972**, *6*, 2579–2595. [10.1103/PhysRevB.6.2579](https://doi.org/10.1103/PhysRevB.6.2579).
61. Guritanu, V.; Goldacker, W.; Bouquet, F.; Wang, Y.; Lortz, R.; Goll, G.; Junod, A. Specific heat of  $\text{Nb}_3\text{Sn}$ : The case for a second energy gap. *Phys. Rev. B* **2004**, *70*, 184526. [10.1103/PhysRevB.70.184526](https://doi.org/10.1103/PhysRevB.70.184526).
62. Orlando, T. P.; McNiff, E. J. Jr.; Foner, S.; Beasley, M.R. Critical fields, Pauli paramagnetic limiting, and material parameters of  $\text{Nb}_3\text{Sn}$  and  $\text{V}_3\text{Si}$ . *Phys Rev B* **1979**, *19*, 4545–4561. [10.1103/PhysRevB.19.4545](https://doi.org/10.1103/PhysRevB.19.4545).
63. Zhang, R.; Gao, P.; Wang, X.; Zhou, Y. First-principles study on elastic and superconducting properties of  $\text{Nb}_3\text{Sn}$  and  $\text{Nb}_3\text{Al}$  under hydrostatic pressure. *AIP Advances* **2015**, *5*, 107233. [10.1063/1.4935099](https://doi.org/10.1063/1.4935099).
64. Junod, A.; Muller, J. Comment on specific heat of a transforming  $\text{V}_3\text{Si}$  crystal. *Solid State Communications* **1980**, *36*, 721–724. [10.1016/0038-1098\(80\)90217-3](https://doi.org/10.1016/0038-1098(80)90217-3).

65. Yamashita, A.; Matsuda, T. D.; Mizuguchi, Y. Synthesis of new high-entropy alloy-type Nb<sub>3</sub>(Al, Sn, Ge, Ga, Si) superconductors. *Journal of Alloys and Compounds* **2021**, *868*, 159233. 10.1016/j.jallcom.2021.159233.
66. Winterlik, J.; Fecher, G. H.; Felser, C.; Jourdan, M.; Grube, K.; Hardy, F.; von Löhneysen, H.; Holman, K. L.; Cava, R. J. Ni-based superconductor: Heusler compound ZrNi<sub>2</sub>Ga. *Phys. Rev. B* **2008**, *78*, 184506. 10.1103/PhysRevB.78.184506.
67. Klimczuk, T.; Wang, C. H.; Gofryk, K.; Ronning, F.; Winterlik, J.; Fecher, G. H.; Griveau, J.-C.; Colineau, E.; Felser, C.; Thompson, J. D.; Safarik, D. J.; Cava, R. J. Superconductivity in the Heusler family of intermetallics. *Phys. Rev. B* **2012**, *85*, 174505. 10.1103/PhysRevB.85.174505.
68. Singh, D.; Barker, J. A. T.; Thamizhavel, A.; Hillier, A. D.; Paul, D. McK.; Singh, R. P. Superconducting properties and  $\mu$ SR Study of the noncentrosymmetric superconductor Nb<sub>0.5</sub>Os<sub>0.5</sub>. *J. Phys.: Condens. Matter* **2018**, *30*, 075601. 10.1088/1361-648X/aaa376.
69. Karki, A. B.; Xiong, Y. M.; Vekhter, I.; Browne, D.; Adams, P.W.; Young, D. P.; Thomas, K.R.; Chan, J. Y.; Kim, H.; Prozorov, R. Structure and physical properties of the noncentrosymmetric superconductor Mo<sub>3</sub>Al<sub>2</sub>C. *Phys. Rev. B* **2010**, *82*, 064512. 10.1103/PhysRevB.82.064512.
70. Górnicka, K.; Gui, X.; Wiendlocha, B.; Nguyen, L. T.; Xie, W.; Cava, R. J.; Klimczuk, T. NbIr<sub>2</sub>B<sub>2</sub> and TaIr<sub>2</sub>B<sub>2</sub> – New low symmetry noncentrosymmetric superconductors with strong spin-orbit coupling. *Adv. Funct. Mater.* **2020**, *31*, 2007960. 10.1002/adfm.202007960.
71. Barker, J. A. T., Breen, B. D.; Hanson, R.; Hillier, A. D.; Lees, M. R.; Balakrishnan, G.; Paul, D. McK.; Singh, R. P. Superconducting and normal-state properties of the noncentrosymmetric superconductor Re<sub>3</sub>Ta. *Phys. Rev. B* **2018**, *98*, 104506. 10.1103/PhysRevB.98.104506.
72. Gong, C.; Wang, Q.; Wang, S.; Lei, H. Superconducting properties of MgCu<sub>2</sub>-type Laves phase compounds SrRh<sub>2</sub> and BaRh<sub>2</sub>. *J. Phys.: Condens. Matter* **2020**, *32*, 295601. 10.1088/1361-648X/ab7c12.
73. Gutowska, S.; Górnicka, K.; Wójcik, P.; Klimczuk, T.; Wiendlocha, B. Strong-coupling superconductivity of SrIr<sub>2</sub> and SrRh<sub>2</sub>: Phonon engineering of metallic Ir and Rh. *Phys. Rev. B* **2021**, *104*, 054505. 10.1103/PhysRevB.104.054505.
74. Horie, R.; Horigane, K.; Nishiyama, S.; Akimitsu, M.; Kobayashi, K.; Onari, S.; Kambe, T.; Kubozono, Y.; Akimitsu, J. Superconductivity in 5d transition metal Laves phase SrIr<sub>2</sub>. *J. Phys.: Condens. Matter* **2020**, *32*, 175703. 10.1088/1361-648X/ab6a2e.
75. Mao, Z. Q.; Rosario, M. M.; Nelson, K. D.; Wu, K.; Deac, I. G.; Schiffer, P.; Liu, Y.; He, T.; Regan, K. A.; Cava, R. J. Experimental determination of superconducting parameters for the intermetallic perovskite superconductor MgCNi<sub>3</sub>. *Phys. Rev. B* **2003**, *67*, 094502. 10.1103/PhysRevB.67.094502.
76. Rzyńska, Z.; Chamorro, J. R.; McQueen, T. M.; Wiśniewski, P.; Kaczorowski, D.; Xie, W.; Cava, R. J.; Klimczuk, T.; Winiarski, M. J. RuAl<sub>6</sub> –An endohedral aluminide superconductor. *Chem. Mater.* **2020**, *32*, 3805–3812. 10.1021/acs.chemmater.9b05277.
77. Langenberg, E.; Ferreiro-Vila, E.; Leborán, V.; Fumega, A. O.; Pardo, V.; Rivadulla, F. Analysis of the temperature dependence of the thermal conductivity of insulating single crystal oxides. *APL Materials* **2016**, *4*, 104815. 10.1063/1.4966220.
78. Adroja, D.; Bhattacharyya, A.; Biswas, P. K.; Smidman, M.; Hillier, A. D.; Mao, H.; Luo, H.; Cao, G.-H.; Wang, Z.; Wang, C. Multigap superconductivity in ThAsFeN investigated using  $\mu$ SR measurements. *Phys. Rev. B* **2017**, *96*, 144502. 10.1103/PhysRevB.96.144502.
79. Albedah, M. A.; Nejadsattari, F.; Stadnik, Z. M.; Wang, Z.-C.; Wang, C.; Cao, G.H. Absence of the stripe antiferromagnetic order in the new 30 K superconductor ThFeAsN. *Journal of Alloys and Compounds* **2017**, *695*, 1128–1136. 10.1016/j.jallcom.2016.10.239.
80. Bhattacharyya, A.; Adroja, D.T.; Smidman, M.; Anand, V. K. A brief review on  $\mu$ SR studies of unconventional Fe- and Cr-based superconductors. *Sci. China Phys. Mech. Astron.* **2018**, *61*, 127402. 10.1007/s11433-018-9292-0.
81. Sonier, J. E.; Sabok-Sayr, S. A.; Callaghan, F. D.; Kaiser, C. V.; Pacradouni, V.; Brewer, J. H.; Stubbs, S. L.; Hardy, W. N.; Bonn, D. A.; Liang, R.; Atkinson, W. A. Hole-doping dependence of the magnetic penetration depth and vortex core size in YBa<sub>2</sub>Cu<sub>3</sub>O<sub>y</sub>: Evidence for stripe correlations near 1/8 hole doping. *Phys. Rev. B* **2007**, *76*, 134518. 10.1103/PhysRevB.76.134518.
82. Kiefl, R.F.; Hossain, M. D.; Wojek, B. M.; Dunsiger, S. R.; Morris, G. D.; Prokscha, T.; Salman, Z.; Baglo, Bonn, D. A.; Liang, R.; et. al. Direct measurement of the London penetration depth in YBa<sub>2</sub>Cu<sub>3</sub>O<sub>6.92</sub> using low-energy  $\mu$ SR. *Phys. Rev. B* **2010**, *81*, 180502(R). 10.1103/PhysRevB.81.180502.
83. Uemura, Y. J. Muon spin relaxation studies on high-  $T_c$  organic, heavy-fermion, and Chevrel phase superconductors. *Physica B* **1991**, *169*, 99–106. 10.1016/0921-4526(91)90214-Y.
84. Sebastian, S. E.; Harrison, N.; Lonzarich, G. G. Towards resolution of the Fermi surface in underdoped high-  $T_c$  superconductors. *Rep. Prog. Phys.* **2012**, *75*, 102501. 10.1088/0034-4885/75/10/102501.
85. Hsua, Y.-T.; Hartstein, M.; Davies, A. J.; Hickey, A. J.; Chan, M. K.; Porras, J.; Loew, T.; Taylor, S. V.; Liua, H.; Eaton, A. G.; et. al. Unconventional quantum vortex matter state hosts quantum oscillations in the underdoped high-temperature cuprate superconductors. *PNAS* **2021**, *118*, e2021216118. 10.1073/pnas.2021216118.

86. Padilla, W. J.; Lee, Y. S.; Dumm, M.; Blumberg, G.; Ono, S.; Segawa, K.; Komiya, S.; Ando, Y.; Basov, D. N. Constant effective mass across the phase diagram of high- $T_c$  cuprates. *Phys. Rev. B* **2005**, *72*, 060511(R). 10.1103/PhysRevB.72.060511.
87. Ledbetter, H. Dependence of on Debye temperature  $\Theta_D$  for various cuprates. *Physica C* **1994**, *235-240*, 1325-1326. 10.1016/0921-4534(94)91887-2.
88. Talantsev, E. F.; Tallon, J. L. Universal self-field critical current for thin-film superconductors. *Nat. Comms.* **2015**, *6*, 7820. 10.1038/ncomms8820.
89. Talantsev, E.; Crump, W. P.; Tallon, J. L. Thermodynamic parameters of single- or multi-band superconductors derived from self-field critical currents. *Annalen der Physik* **2017**, *529*, 1700197. 10.1002/andp.201700197.
90. Wagner, P.; Hillmer, F.; Frey, U.; Adrian, H. Thermally activated flux movement and critical transport current density in epitaxial  $\text{Bi}_2\text{Sr}_2\text{CaCu}_2\text{O}_{8+\delta}$  films. *Phys. Rev. B* **1994**, *49*, 13184. 10.1103/PhysRevB.49.13184.
91. Holstein, W. L.; Wilker, C.; Laubacher, D. B.; Face, D. W.; Pang, P.; Warrington, M. S.; Carter, C. F.; Parisi, L. A. Critical current density and resistivity measurements for long patterned lines in  $\text{Tl}_2\text{Ba}_2\text{CaCu}_2\text{O}_8$  thin films. *Journal of Applied Physics* **1993**, *74*, 1426-1430. 10.1063/1.354902.
92. Krusin-Elbaum, L.; Tsuei, C. C.; Gupta, A. High current densities above 100 K in the high-temperature superconductor  $\text{HgBa}_2\text{CaCu}_2\text{O}_{6+\delta}$ . *Nature* **1995**, *373*, 679-681. 10.1038/373679a0.
93. Hänisch, J.; Attenberger, A.; Holzapfel, B.; Schultz, L. Electrical transport properties of  $\text{Bi}_2\text{Sr}_2\text{Ca}_2\text{Cu}_3\text{O}_{10+\delta}$  thin film [001] tilt grain boundaries. *Phys. Rev. B* **2002**, *65*, 052507. 10.1103/PhysRevB.65.052507.
94. Cao, Y.; Fatemi, V.; Fang, S.; Watanabe, K.; Taniguchi, T.; Kaxiras, E. and Jarillo-Herrero, P. Unconventional superconductivity in magic-angle graphene superlattices. *Nature* **2018**, *556*, 43-50. 10.1038/nature26160
95. Talantsev, E. F.; Mataira, R. C.; Crump, W. P. Classifying superconductivity in Moiré graphene superlattices. *Scientific Reports* **2020**, *10*, 212. 10.1038/s41598-019-57055-w.
96. Cucemasov, A. I.; Nika, D. L.; Balandin, A. A. Engineering of the thermodynamic properties of bilayer graphene by atomic plane rotations: the role of the out-of-plane phonons. *Nanoscale* **2015**, *7*, 12851. 10.1039/C5NR03579A.
97. Eremets, M. I.; Shimizu, K.; Kobayashi, T. C.; Amaya, K. Metallic CsI at pressures of up to 220 gigapascals. *Science* **1998**, *281*, 1333-1335. 10.1126/science.281.5381.1333.
98. Talantsev, E. F. Fermi-liquid nonadiabatic highly compressed cesium iodide superconductor. *Condensed Matter* **2022**, *7*(4), 65. 10.3390/condmat7040065.
99. Talantsev, E. F. The dominance of non-electron-phonon charge carrier interaction in highly-compressed superhydrides. *Supercond. Sci. Technol.* **2021**, *34*, 115001. 10.1088/1361-6668/ac19f3.
100. Talantsev, E. F. Classifying superconductivity in compressed  $\text{H}_3\text{S}$ . *Modern Physics Letters B* **2019**, *33*, (17), 1950195. 10.1142/S0217984919501951.
101. Talantsev, E. F. Electron-phonon coupling constant and BCS ratios in  $\text{LaH}_{10-y}$  doped with magnetic rare-earth element. *Supercond. Sci. Technol.* **2022**, *35*, 095008. 10.1088/1361-6668/ac7d78.
102. Shimizu, K.; Suhara, K.; Ikumo, M.; Eremets, M. I.; Amaya, K. Superconductivity in oxygen. *Nature* **1998**, *393*, 767-769.
103. Talantsev, E. F. An approach to identifying unconventional superconductivity in highly compressed superconductors. *Supercond. Sci. Technol.* **2020**, *33*, 124001. 10.1088/1361-6668/abb11a.
104. Talantsev, E. F.; Crump, W. P. Weak-links criterion for pnictide and cuprate superconductors. *Superconductors Science and Technology* **2018**, *31*, 124001. 10.1088/1361-6668/aae50a.
105. Paturi, P.; and Huhtinen, H. Roles of electron mean free path and flux pinning in optimizing the critical current in YBCO superconductors. *Supercond. Sci. Technol.* **2022**, *35*, 065007. 10.1088/1361-6668/ac68a5.
106. Hirsch, J. E.; Marsiglio, F. Clear evidence against superconductivity in hydrides under high pressure. *Matter Radiat. Extremes* **2022**, *7*, 058401. 10.1063/5.0091404.
107. Hirsch, J. E.; Marsiglio, F. Evidence against superconductivity in flux trapping experiments on hydrides under high pressure. *Journal of Superconductivity and Novel Magnetism* **2022**, *35*, 3141-3145. 10.1007/s10948-022-06365-8.
108. Hirsch, J. E. Hole superconductivity xOr hot hydride superconductivity. *J. Appl. Phys.* **2021**, *130*, 181102. 10.1063/5.0071158.
109. Hirsch, J. E.; Marsiglio, F. Nonstandard superconductivity or no superconductivity in hydrides under high pressure. *Phys. Rev. B* **2021**, *103*, 134505. 10.1103/PhysRevB.103.134505.
110. Talantsev, E. F.; Stolze, K. Resistive transition of hydrogen-rich superconductors. *Supercond. Sci. Technol.* **2021**, *34*, 064001. 10.1088/1361-6668/abf23c.
111. Hirsch, J. E.; Marsiglio, F. Hole superconductivity in  $\text{H}_2\text{S}$  and other sulfides under high pressure. *Physica C* **2015**, *511*, 45-49. 10.1016/j.physc.2015.01.008.
112. Hirsch, J. E. Hole superconductivity. *Physica C* **1989**, *134*, 451-455. 10.1103/PhysRevB.41.6435. 10.1016/0375-9601(89)90370-8.

113. Marsiglio F.; Hirsch, J. E. Hole superconductivity and the high- $T_c$  oxides. *Phys. Rev. B* **1990**, *41*, 6435-6456. 10.1103/PhysRevB.41.6435.
114. Hirsch, J. E. Why only hole conductors can be superconductors. *Proc. SPIE 10105, Oxide-based Materials and Devices VIII*, 101051V (March 7, 2017). 10.1117/12.2269644.
115. Souza, T. X. R.; Marsiglio, F. Systematic study of the superconducting critical temperature in two- and three-dimensional tight-binding models: A possible scenario for superconducting  $H_3S$ . *Phys. Rev. B* **2016**, *94*, 184509. 10.1103/PhysRevB.94.184509.
116. Souza, T. X. R.; Marsiglio, F. The possible role of van Hove singularities in the high of superconducting  $H_3S$ . *International Journal of Modern Physics B* **2017**, *31*, 1745003. 10.1142/S0217979217450035.
117. Hirsch, J. Towards an understanding of hole superconductivity. In: Bussmann-Holder, A., Keller, H., Bianconi, A. (eds) High-Tc Copper Oxide Superconductors and Related Novel Materials. Springer Series in Materials Science, vol 255. Springer, Cham., **2017**. 10.1007/978-3-319-52675-1\_9.
118. Charnukha, A. Optical conductivity of iron-based superconductors. *J. Phys.: Condens. Matter* **2014**, *26*, 253203. 10.1088/0953-8984/26/25/253203.
119. Williamson, P. Take the time and effort to correct misinformation. *Nature* **2016**, *540*, 171. 10.1038/540171a.